THE IMPACT OF GAS BULK ROTATION ON THE LYMAN-α LINE

Nicolas Garavito-Camargo[1], Jaime E. Forero-Romero[1], Mark Dijkstra[2]
Submitted for publication in ApJ

ABSTRACT

Rotation is present in the gas kinematics of galaxies up to the highest redshifts. In this paper we present for the first time radiative transfer calculations that show the impact of gas bulk rotation on the morphology of the Lyman α line. To this end we model a galaxy as an homogeneous sphere composed as an homogeneous mixture of dust and hydrogen at a constant temperature. These spheres have a solid-body rotation with linear velocities at the surface in the range $0 - 300$ km s^{-1} and neutral hydrogen optical depths in the range $\tau_{\rm H} = 10^5 - 10^7$. We consider radiation sources both in the center of the rotating cloud and also homogeneously distributed in the volume. We find that higher rotational velocities increase the width of each peak in the outgoing line profile while it also increases the amount of Lyman alpha photons escaping in the line center. This trends makes that for high rotational velocities and large Hydrogen optical depths the double peak of the line tends to be erased an be replaced by a single peak a the line center. This trend is more pronounced for radiation sources homogeneously distributed. Concerning the escape fraction we find that rotation does not have any effect, provided that all the sources are centrally emitted. However, in the case of homogeneously emittedsources we measure an increase of about a factor of 2 in the escape fraction for higher rotational velocity values. This work shows that gas bulk rotation has a non negligible impact on the shape of the Lyman α line.

Subject headings: galaxies: high-redshift,galaxies: star formation, line: formation

1. INTRODUCTION

The detection of strong Lyα emission lines has become an essential method in extragalactic astronomy to find distant star-forming galaxies (Partridge & Peebles 1967; Rhoads et al. 2000; Gawiser et al. 2007; Koehler et al. 2007; Ouchi et al. 2008; Yamada et al. 2012; Schenker et al. 2012). The galaxies detected using this method receive the name of Lyα emitters (LAEs). A detailed examination of this galaxy population has diverse implications for galaxy formation, reionization and the large scale structure of the Universe. Attempts to fully exploit the physical information included in the Lyα line require an understading of all the physical factors involved in shaping the line. Due to the resonant nature of this line, these physical factors include temperature, density and bulk velocity field of the neutral Hydrogen in the emitting galaxy and its surroundings.

A basic understanding for the quantitative behaviour of the Lyα line has been reached through analytical studies in the case of a static configurations, such as uniform slabs (Harrington 1973; Neufeld 1990) and uniform spheres (Dijkstra et al. 2006). Analytical studies of configurations including some kind of bulk flow only include the case of a sphere with a Hubble like expansion flow (Loeb & Rybicki 1999).

A more detailed quantification of the Lyα line has been reached using Monte Carlo simulations (Auer 1968; Avery & House 1968; Adams 1972). In the last two decades these studies have become more popular due to the availability of computing power. Early into the 21st century the first studies focused on on homogeneous and static media (Ahn et al. 2000, 2001; Zheng & Miralda-Escudé

2002). Later on the effects of clumpy media (Hansen & Oh 2006) and expanding/contracting shell/spherical geometries started to be studied (Verhamme et al. 2006; Dijkstra et al. 2006). Similar codes have applied these results to semi-analytical models of galaxy formation (Orsi et al. 2012) and results of large hydrodynamical simulations (Forero-Romero et al. 2011, 2012; Behrens & Niemeyer 2013). Recently Monte Carlo codes have also been applied to the results of high resolution hydrodynamical simulations (Laursen et al. 2009; Barnes et al. 2011; Verhamme et al. 2012; Yajima et al. 2012). Recent developments have been focused on the study of clumpy outflows (Dijkstra & Kramer 2012)and anisotropic velocity configurations (Zheng & Wallace 2013).

The recent studies of galaxies in hydrodynamical simulations (Laursen et al. 2009; Barnes et al. 2011; Verhamme et al. 2012; Yajima et al. 2012) have all shown systematic variations in the Lyα line with the viewing angle. These variations are a complex superpositions of anisotropic density configurations (i.e. edge-on vs. face-on view of a galaxy), the inflows observaed by gas cooling and the outflows included in the supernova feedback process of the simulation. These bulk flows physically correspond to the circumgalactic and intergalactic medium (CGM and IGM). These effects have been systematically studied different anisotropic models of hydrogen clouds varying the density and wind characteristics (Zheng & Wallace 2013).

However, in all these systematics efforts the effect of rotation, which is an ubiquitous feature in galaxies, has not been systematically studied. The processing of the Lyα photons in a rotating interstellar medium (ISM) must have an impact in the line morphology. It is necessary to investigate to what extent bulk gas rotation has an measurable impact in the Lyα alpha line.

[1] Departamento de Física, Universidad de los Andes, Cra. 1 No. 18A-10, Edificio Ip, Bogotá, Colombia
[2] _

Performing that study is the main goal of this paper. We investigate for the first time the impact of rotation on the morphology of the Lyman α line. We focus on a simplified system, a spherical gas cloud with homogeneous density and solid body rotation. We focus our study on the line morphology, anisotropic integrated emission and the escape fraction in the presence of dust. We base our work on two independent Monte Carlo based radiative transfer codes CLARA (Forero-Romero et al. 2011) and XX (Dijkstra & Kramer 2012) .

This paper is paper is structured as follows. In §2 we present the implementation of bulk rotation into the Monte Carlo codes, paying special attention to coordinate definitions. There we also list the different physical parementers in the simulated grid of models. In the next section we present the results of the simulations, with special detail to quantities in the line that show a clear evolution as a function of the cloud's rotational velocity. In §**??** we discuss the implications of our results in the interpretation of LAEs observations and further refinements that can be implemented in the theoretical modelling of the Lyα line. In the last section we preset our conclusiones.

In this paper we express a photon's frequency in terms of the dimensionless variable $x \equiv (\nu - \nu_a)/\Delta\nu_\alpha$, where $\nu_\alpha = 2.46 \times 10^{15}$ Hz is the Lyα resonance frequency, $\Delta\nu_\alpha \equiv \nu_\alpha\sqrt{2kT/m_pc^2} \equiv \nu_a v_{\rm th}$ is the doppler broadening of the line which depends on the neutral gas temperature T scattering the radiation or equivalently the thermal velocity $v_{\rm th}$ of the atoms.

2. MODELS OF BULK GAS ROTATION

Describing the kinematics of gas rotation in all generality is a complex task, specially at high redshifts where there is still missing a thorough observational account of rotation in galaxies beyond $z > 1.0$. Furthermore, at low redshifts it has been observed a great variation in the shape of the rotation curve as observed in HI emission as a function of the distance to the galaxy center. However there are two features that are observed very often. First, in the central region the velocity increases proportional to the radius, following the behaviour in a body with solid rotation. Second, beyond a certain radius the rotation curve tends to flatten.

An ab-initio description of realistic rotation curves in simulations depends on having access to the dynamic evolution of all mass components in the galaxy: stars, gas and dark matter. Such level of realism is extremely complex to achieve, specially if one wants to get a systematic description based on statistics of simulated objects.

Following the tradition of studies of Lymanα emitting systems, we implement a model with a simplified geometry and gas distribution. We assume that the gas is homogeneously distributed in a sphere that rotates as a solid body with constant angular velocity. This simple model will contain only one parameter: the linear velocity at the sphere's surface, $V_{\rm max}$.

2.1. *Detailed Implementation of Rotation*

In the MonteCarlo code we define a cartesian coordinate system to describe the position of each photon. The origin of this system coincides with the center of the sphere and the rotation axis is defined to be z-axis. With

Physical Parameter (units)	Symbol	Values
Velocity (km s^{-1})	$V_{\rm max}$	0, 50, 100, 200, 300
Hydrogen Optical Depth	τ_H	10^5, 10^6, 10^7
Dust Optical Depth	τ_a	0,1
Photons Distributions		Central, Homogeneous

TABLE 1
LIST OF THE PHYSICAL PARAMETERS THAT DEFINE THE SPHERICAL MODELS SIMULATED IN OUR MONTE CARLO CALCULATIONS. FOR EACH PARAMETER WE VARY THE VALUES IN THE RANGE LISTED IN THE LAST COLUMN. TAKIG INTO ACCOUNT ALL THE POSSIBLE COMBINATIONS WE END UP WITH 60 DIFFERENT MODELS.

this choice, the components of the gas bulk velocity field, $\vec{v} = v_x\hat{i} + v_y\hat{j} + v_z\hat{k}$, can be written as

$$v_x = -\frac{y}{R}V_{\rm max}, \tag{1}$$

$$v_y = \frac{x}{R}V_{\rm max}, \tag{2}$$

$$v_z = 0, \tag{3}$$

where R is the radius of the sphere and $V_{\rm max}$ is the linear velocity at the sphere's surface. The minus/plus sign in the x/y-component of the velocity indicates the direction of rotation. In this case we take the angular velocity in the same direction as the $\hat{k}$ unit vector. With these definitions we can write the angular velocity as $\omega = V_{\rm max}/R$.

For each photon in the simulation we have its initial position inside the sphere, direction of propagation $\hat{k}_{in}$ and reduced frequency x_{in}. The photon's propagation stops once they cross the surface of the sphere. At this point we store the position, the outgoing direction of propagation $\hat{k}_{out}$ and the reduced frequency x_{out}. We define the angle Θ by $\cos\Theta = \hat{k} \cdot \hat{k}_{out}$, that is the polar angle of the outgoing photon with respect to the z axis. Following Zheng & Wallace (2013) we make the study of the anisotropic emission in terms of this angle Θ.

2.2. *Grid of Simulated Galaxies*

In the Monte Carlo calculations we follow the propagation of $N_\gamma = 10^5$ numerical photons through different spherical galaxies. For each galaxy we vary at least one of the following parameters: the maximum rotational velocity $V_{\rm max}$, the hydrogen optical depth τ_H, the dust optical depth τ_a and the initial distribution of photons with respect to the gas. There are in total 60 models combining all the input parameters. Table 1 presents a summary of all the models.

Additionally, we have used two independently developed Monte Carlo codes (Forero-Romero et al. 2011; Dijkstra & Kramer 2012) to perform the calculations of the non-dusty models. The results we report here are robust in the sense that they are obtained by both codes.

3. RESULTS

The central result of this paper is summarized in Figure 1. It shows the considerable impact of rotation on the morphology of the emergent Lyα line. Both panels in the Figure focus on the results for $\tau_H = 10^7$, showing that the influence of rotation is present both when the photons are either homogeneously or centrally initialized over the gas volume.
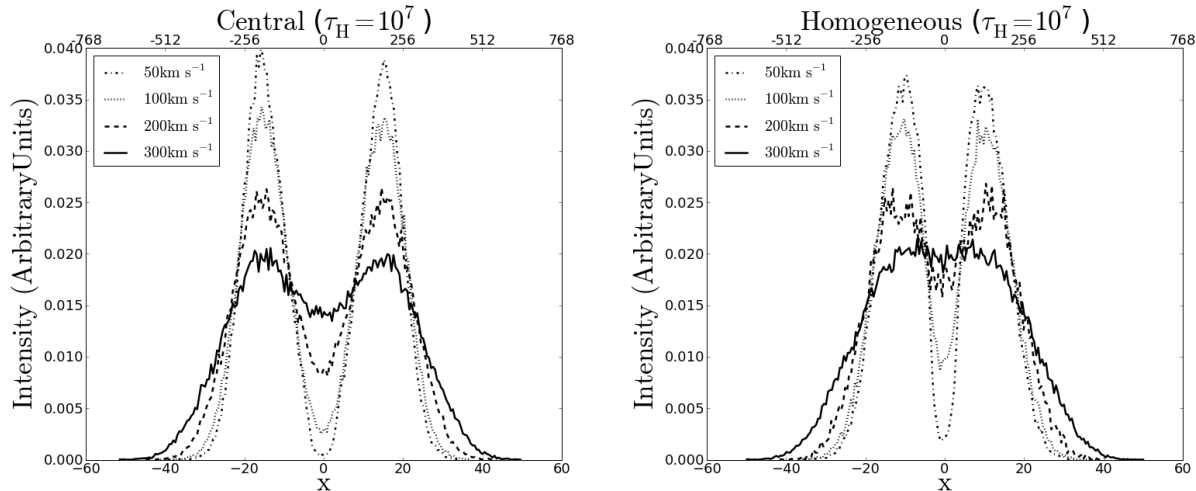
FIG. 1.— Shape of the Lyα line for different velocities rotational velocities for spherical distributions with $\tau_H = 10^7$. The left (right) panel shows the central (homogeneous) photon distribution. All photons were taken into account regardless of their final direction of propagation.
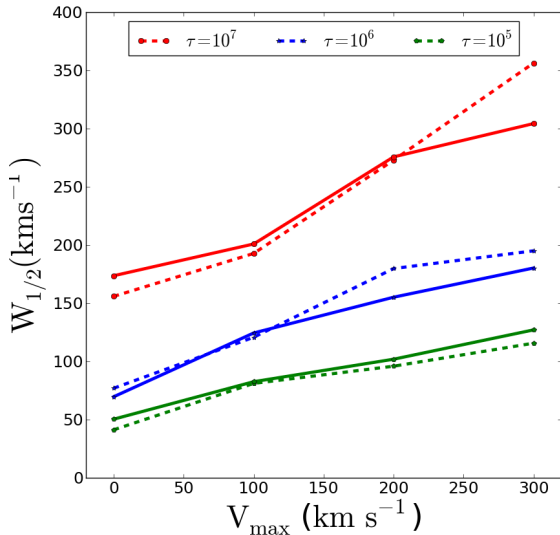

FIG. 2.— Half-width for the non-dusty models as a function of rotational velocity $V_{\max}$. Continuous (dashed) lines correspond to homogeneous (central) source distributions.

FIG. 3.— Position of the peak maxima as a function of rotational velocity $V_{\max}$. Continuous (dashed) lines correspond to homogeneous (central) source distributions. A value of $x_{\max} = 0$ indicates that line becomes single peaked.

In the following subsections we characterize the line morphology by the half-width at half intensity and the peak maxima. In order to interpret the morphological changes in the line we also report the median number of scatter for each Lyα photon in the simulation. For the models where dust is included we measure the bulk escape fraction as a function of rotational velocity. Finally, we make an estimate of the anisotriopic emission of the models in comparison with static spheres.

3.1. Line width and peak maxima

The first quantitative conclusion of the effect of rotation in the Lyα line is that double peaks broaden and reduce their intensity while the line center rises. This produces the impression that, as the rotational velocity increases, the double peaks are merged into a single broad emission peak. This is most evident at the highest rotational velocities for the homogeneously distributed sources (right panel in Figure 1).
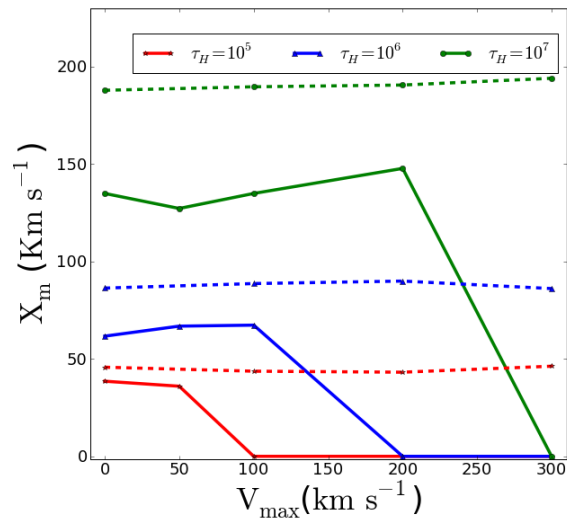
To quantify the line broadening we use a modified version of the full width at half maximum (FWHM). We measure it only for half of the line, $W_{1/2}$. This definition allows us to quantify the line width and see the transition from double to single peak emission. In the case of double peaked emission $W_{1/2}$ corresponds to the width of a single peak, while in the extreme case of high rotational velocities, when the double peak is erased, it simply correspond to half FWHM.

Figure 2 shows how $W_{1/2}$ increases with rotational velocity. Continuous (dashed) lines connect the results for homogeneous (central) source distribution. For the temperature $T = 10^4$K used in our radiative transfer calculations the thermal velocity is $v_{th} = 12.8\,\mathrm{km\,s^{-1}}$. For a model with τ_H it means that the half-width can increase up to $350\,\mathrm{km\,s^{-1}}$ (at $V_{\max} = 300\,\mathrm{km\,s^{-1}}$) compared to a

half-width of $150\,\mathrm{km\,s^{-1}}$ in the static case.

Figure 3 shows the position for the peak maxima as a function of the rotational velocity $V_{\max}$. This Figure clearly shows that in the case of central distributed sources there is barely any change with rotational velocity in the range of explored parameters. However, in the case of homogeneously emitted sources the maxima position remain close to constant until beyond some velocity threshold the line becomes single peaked with $x_{\max} = 0$ km $\mathrm{s^{-1}}$.

The transition to a single peak line seems to occur for systems where it becomes easier for the bulk of the photons to escape with the lowest number of scatterings possible, allowing them not to move very far from the center of the line. This might explain how the single peak stage is easily achieved in the homogeneous source distribution. In this case there is a fraction of the photons that are inside a photosphere region with $\tau_{H,r} \ll \tau_H$ where $\tau_{H,r}$ is the optical depth from the radius of emission to the sphere's surface. This conditions allows the photons to escape with much less scatterings compared to the photons emitted at the very center of the sphere. In turn, it gives the photons less scatterings to be placed far from the line center.

Increasing the rotational velocity $V_{\max}$ reduces the optical depth making the photosphere region effectively larger, increasing the number of photons escaping close to the lines's center. In our models we find the following correspondence between the optical depth $\tau_H = \{10^5, 10^6, 10^7\}$ and the transitional velocities $V_{\mathrm{trans}} = \{50 - 100\,\mathrm{km\,s^{-1}}, 100 - 200\,\mathrm{km\,s^{-1}}, 200 - 300\,\mathrm{km\,s^{-1}}\}$ which can only be constrained to be in the range of velocities in the models that gave a $x_{\max} \neq 0$ and $x_{\max} = 0$.

For the central emission the transition to a single peak is never completed in the range of parameters explored here. The nonappearence of a single peak phase can be in part explained to the absence of a photosphere, as is the case in the homogeneous distribution. Nevertheless, there is a rise in the intensity at the line center as the rotational velocity increases. This hints that the encounters with a nonstatic medium are inefficient in changing a photons' frequency outside the line center.

In the next section we quantify the number of scatterings and explore to what extent this is related to the emergence of single peak.

3.2. Average Number of Scatterings

The number of times that a Lyα photon is absorbed and re-emitted is connected to the final frequency that it can have after escaping the galaxy. In the case of static gas geometries, a large value of the optical depth is immediately followed by a high number of scatterings. In turn a large optical depth increases the probability that a Lyα photon to be found far from the center of the line. In this case, the peak maxima shift away form the line center as the amount of neutral hydrogen increases.

In Figure 4 we show the average number of scatterings $\langle N_{\mathrm{scatt}} \rangle$ as a function of the rotational velocity $V_{\max}$. For the central distributions we find that there is not a significant change for increasing rotational velocities, $\langle N_{\mathrm{scatt}} \rangle$ changes less than 0.5% for different velocities. In this case we also find that the average number of scatterings is proportional to the opti-
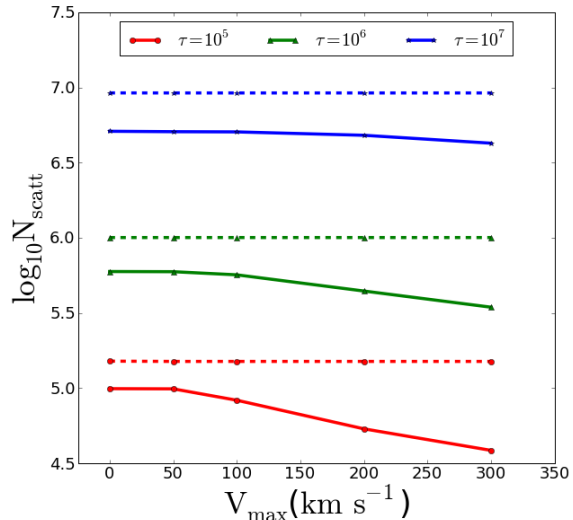

FIG. 4.— Logarithm of the average number of scatterings as function of the velocity. Continuous/dashed lines represent an homogeneous/central distribution of sources.

cal depth, as expected in analogy from the analytic result for the homogeneous infinite-slab $\langle N_{\mathrm{scatt}} \rangle = 1.612\tau_H$ (Adams 1972; Harrington 1973). In our experiments we find that for the static spheres with centraly distributed sources $\langle N_{\mathrm{scatt}} \rangle = (1.50, 1.00, 0.92)\tau_H$. for optical depths $\tau_H = (10^5, 10^6, 10^7)$

Figure 4 shows that for the homogeneous distribution there is a clear decrease of $\langle N_{\mathrm{scatt}} \rangle$ as the $V_{\max}$ increases. This effect more pronounced for the lower values of the optical depth. For $\tau_H = 10^5$ the average number of scatterings decreases by 61% at $V_{\max} = 300\,\mathrm{km\,s^{-1}}$ in comparison to the static case.

The analytic expectation for the slab with homogeneously emitted sources is $\langle N_{\mathrm{scatt}} \rangle = 1.16\tau_H$ (Harrington 1973), a factor of 0.72 lower than the case of the centrally emitted photons. In our case we find that for the static , while for homogeneously distributed source $\langle N_{\mathrm{scatt}} \rangle = (0.99, 0.59, 0.51)\tau_H$, this represents a factor of $(0.66, 0.59, 0.51)$ lower than the centrally emitted photons.

In order to gain a deeper understanding of these results we prepare 2D histograms for the number of scatterings as a function of the outgoing dimensionless frequency x. In Figure 5 we show the results of such histogram in the case $\tau_H = 10^5$ for the static case and $V_{\max} = 300\,\mathrm{km\,s^{-1}}$. The upper (lower) panels show the results for the homogeneous (central) source distribution. The color scale is logarithmic in the number of photons at a certain value $x - N_{\mathrm{scatt}}$. This Figure clearly support our hypothesis about the photosphere in the homogeneous distribution, in this case most of the photons that left with $x \sim 0$ have escaped with less than 10 scatterings, explaining the origin of a single central peak. However, for a central distribution the situation is different. In this case the number of scatterings remains high, on the order of the optical depth, but the two peaks do get closer to each other. In this case the physical picture is that each scattering, due to the bulk velocity of the gas, is inefficient in driving the photon outside the line center.
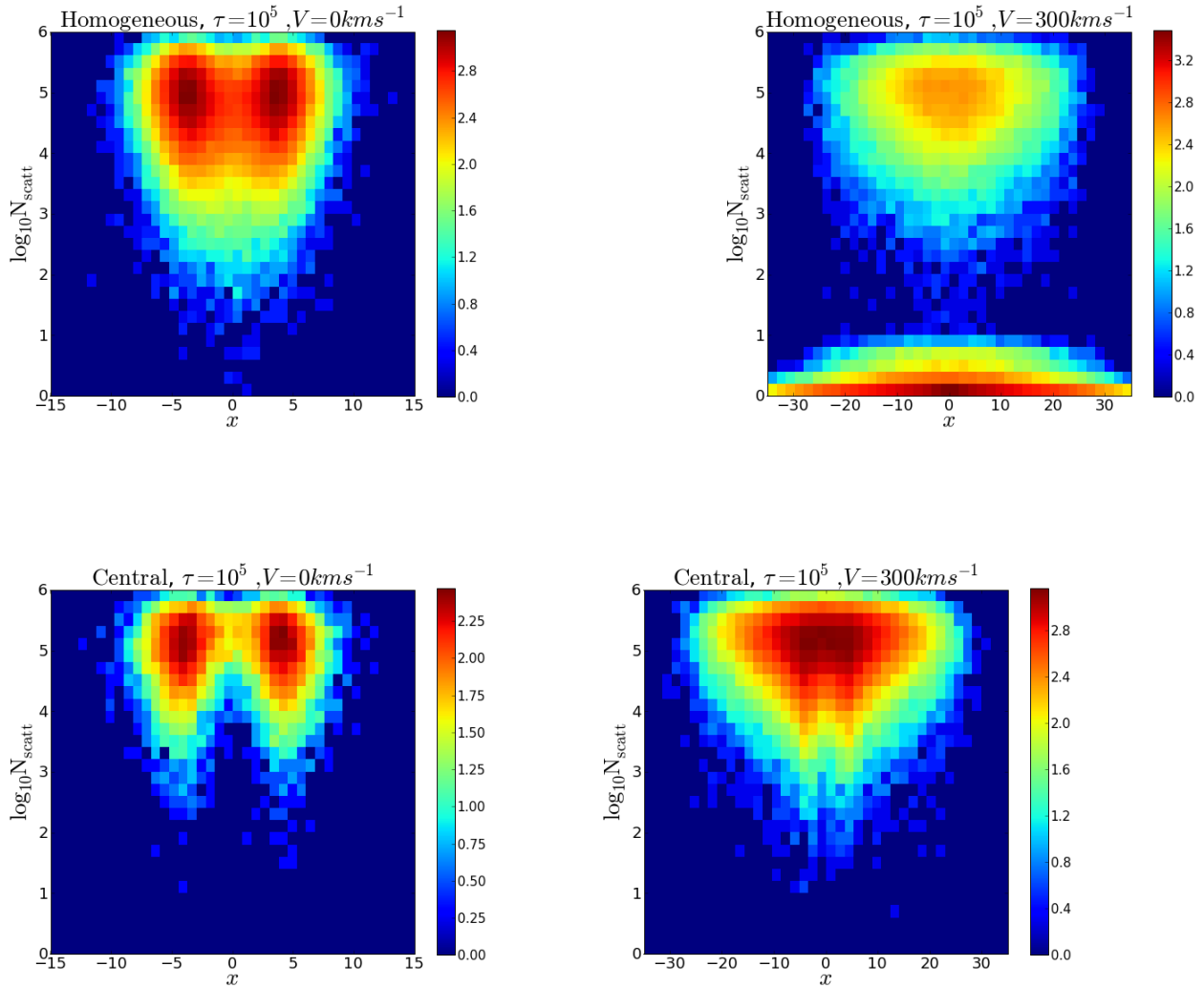
FIG. 5.— 2D histogram of N_{scatt} vs x. The upper (lower) pannels show the homogeneous (central) source distribution. Left corresponds to the static case and the right $V_{max} = 300km/s$. The colour scale is logarithmic on the number of photons with given values of N_{scatt} and x.

3.3. *Dusty Clouds: Escape Fraction*

We also study a dusty cloud configuration to measure the effect of rotation on the escape fraction. We expect that the modified number of scatterings to be reflected in this amount of photons absorbed by dust. Following this line of thought, we do not expect any change in for a dusty cloud with central source of radiation given that the number of scatterings remains close to constant. On the other hand, in the case of an homogeneous radiation source the number of scatterings drops as V_{max} increases, which might be reflected as an increasing escape fraction.

Figure 6 shows the dependence of the escape fraction as a function of the maximum rotational velocity, confirming that our intuitions in this respect is correct. For the central source distribution the escape fraction barely shows any change, while for the homogeneous case there is a clear rise in the escape fraction for high rotational velocities. Rotation has a higher relative impact in the models with low optical depth $\tau_{\mathrm{H}} = 10^5, 10^6$, where it

can raise from $(0.26, 0.28)$ respectively in the static case up to $(0.37, 0.39)$ at $V_{\mathrm{rot}} = 300\,\mathrm{km\,s^{-1}}$.

In Figure 7 we put these results in the context of the analytical solution for the infinite slab (Neufeld 1990). In Neufeld's setup the analytic solution depends solely on the product $(a\tau_{\mathrm{H}})^{1/3}\tau_a$, an approximation that is valid only in the limits $a\tau_{\mathrm{H}} \gg 1$. The dashed lines in Figure 7 correspond to the cases of different velocities. We observe that the escape fraction is higher by factors of $2 - 10$ than the expected values for the slab configuration. We also see that for the lower value $\tau_{\mathrm{H}} = 10^5$ the escape fraction does not increase with respect to the solution for $\tau_{\mathrm{H}} = 10^6$ as expected, however we not that we are in a regime where the condition for the analytic expectations $(a\tau_h \gg 1)$ does not hold.

3.4. *Off-Centered emission*

As we know there is unlikely to find galaxies with radiation sources distributed homogeneously. Most of them

FIG. 6.— Escape fraction as a function of rotational velocity. The continuous (dashed) lines correspond to homogeneous (central) models.
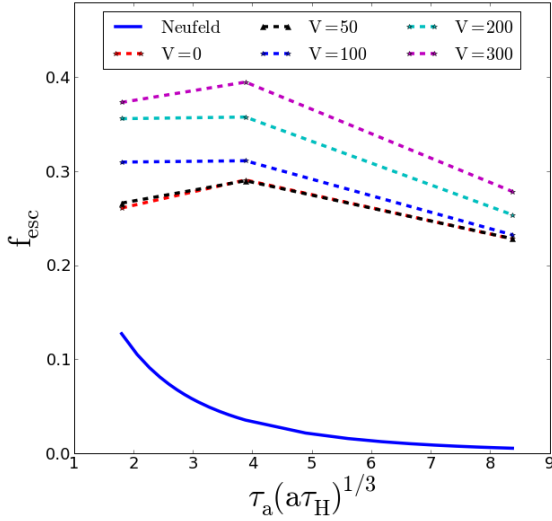

FIG. 7.— Escape fraction as a function of the product $(a\tau_H)^{1/3}\tau_a$. The analytic solution for the infinite is slab shown as a continuous line. Different dashed lines correspond to different rotational velocities.

are in a clumpy distribution (Laursen et al 2013*) which affected the resulting spectra. In order to study an inhomogeneous distribution we set up a model in which we select certain photons that are placed in a specific place but that are not symmetrically distributed Fig. 8 shows the distributions we set up, basically we take photons located in a sphere of $0.5R$ where R is the radii of the homogeneous sphere and we choose two spheres in each side of the $\hat{\mathbf{x}}$ axis two at $0.25R$ and the other two at $0.5R$.

We study the deviations of the received flux on the surface of the sphere. We follow Zheng & Wallace (2013) to estimate the flux seen by an observer located at an angle Θ (distant observer angle) normalized to the isotropic flux:
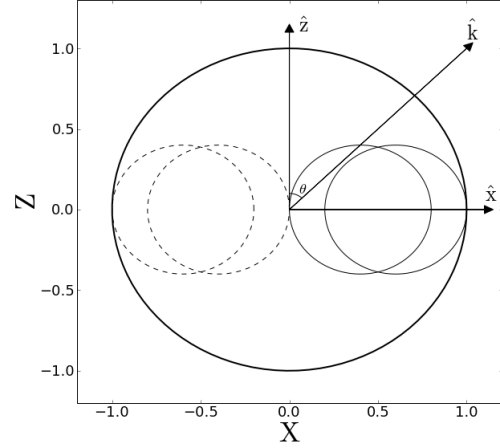

FIG. 8.— The two solid circles show up the photons we select in order to make the anisotropic emission rotation is defined to be z-axis. we also select photons in the negative side of x (dashed circles) in order to see the complete effect of rotation.

$$F(\mu) = \frac{2\Delta N}{N\Delta\mu}, \qquad (4)$$

where $\mu = \cos\Theta$, N is the total number of outgoing photons, ΔN is the number of photons in a angular bin $\Delta\Theta$. This definition satisfies the condition $\int_{-1}^{1} F(\mu)d\mu/2 = 1$.

For the central and homogeneous source distributions we find that observers at different directions do not present an angular dependency, in particular they would infer luminosities different from the isotropical value only at levels $< 3\%$.

But with the set up of the off-center models where the galaxy is rotating around the $\hat{\mathbf{z}}$ axis and the observer is located at $\theta = \pi/2$ we do find and angular dependency for both off-center distributions, this is shown in Fig. 9. The bold line represents an off-center sphere located at $0.25R$ in the homogeneous sphere, while the narrow line shows a sphere located at $-0.25R$. This is done for the model with $\tau = 10^5$ and $V = 50kms^{-1}$, but results with the rest of models show exactly the same trend. We find a high dependency in the viewing angle in particular the flux at $\theta = \pi/2$ is $\simeq 88\%$ stronger than at $\theta = \pi/3$ this have important consequences in observations when galaxies are oriented in random directions which implies that off-center emission is not going to be observed in all the observed galaxies.

The outgoing spectra for two different spheres located at $-0.25R$ and $0.25R$ respectively are shown in Fig. **??**, we have shown this positions because they are most sensitive to the effect of rotation.

There are two new morphological features that off-center emission in rotating galaxies produces. First in some of our models with specific values of velocity and optical depth an asymmetry in the peak heights is presented, those off-center spheres *(put image reference)* located at the positive side of $\hat{\mathbf{x}}$ in Fig.8 present a higher peak in the red-shifted part, while those spheres located at the negative side of $\hat{\mathbf{x}}$ present a higher blue shifted peak, we found that the higher asymmetry is for model with $\tau = 10^7, V = 200kms^{-1}$ where one peak is 20%
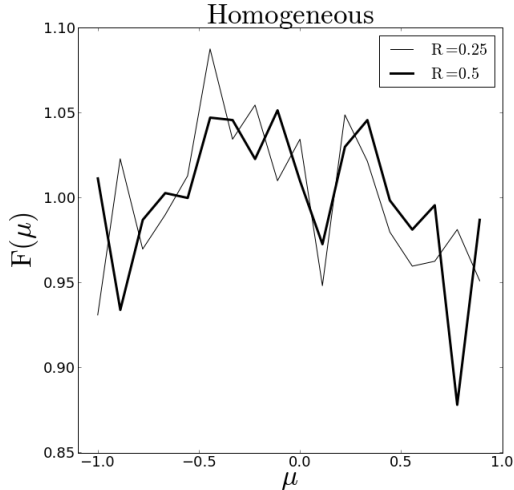
FIG. 9.— Flux angular dependency for Off-center distribution, different line widths illustrate different off-center positions.

higher than the other.

This can be appreciated for both set of spheres at $0.25R$ and $0.5R$, but the effect shows a stronger asymmetry for spheres located at $0.25R$ this due to the fact that photons escaping from this spheres goes through a larger hydrogen medium than photons located in the spheres at $0.5R$.

Also for all the off-center models we found that the $Ly\alpha$ line width ...

Also for photons located in the spheres at $0.5R$, we found that for some models ($\tau = 10^6, V = 100kms^{-1}$ and $\tau = 10^7, V = 200kms^{-1}$) the line presents three peaks (blue-shifted, centered, red-shifted). In order to gain a better interpretation of this three peaks trend we run this models with $N_\gamma = 10^6$.

4. DISCUSSION

Gas bulk rotation has a noticeable effect on the morphology of the $Ly\alpha$ line. In this section we discuss the observational implications of these findings.

We start by a quantitative discussion of the line morphology. Here we follow a classification of $Ly\alpha$ profiles made by Kulas et al. (2012). They presented observational results for star forming galaxies at $z = 2$-3 that showed multiple peaks in their emission. They classified the observed lines into four groups. In Group I the red peak is stronger than the blue, For our porpoises Group II and Group II with the blue peak stronger are the same, Group IV contains double-peak profiles with roughly the same flux and finally group IV present multi-peaked lines.

Neither Group I nor II and III can be fully explained by rotation. However, some comments about some of the galaxies in this groups must be done, in particular for those galaxies in which the flux in between the two peaks is high rotation must be present due to the fact this is until now the most efficient mechanism which produces this effect.

The same argument explained above applies to group IV in which the flux in between of the two peaks is high ($\geq 70\%$ of the highest peak), concerning group V in which multiple-peaks appear homogeneous and central

models can not reproduce such a profiles. While the off-center model could generate similar profiles which is the case of (put reference when the fig. is ready) when tree peaks could appear but with roughly the same flux, this multiple-peaks still need a better comprehension of the gas kinematics.

An other interesting sample of LAEs was presented by Yamada et al. (2012) for 91 LAEs at $z = 3.1$. From that sample 31 LAEs ($\sim 33\%$) present a single peak profile, if this single peak is present an asymmetry it can be explained with the outflow model Verhamme et al. (2008) due to the fact that we don't find any asymmetry due to rotation in both homogeneous and central models, while in the off-center model —. But if it is not the case (put LAEs name for those that do not present asymmetry) now they can be understanding with rotation.

Even in profiles where the double-peaked is presented rotation also could be present as it is seen in Fig.1 where rotation makes that the central part of the line is higher than in profiles where there is no rotation. This could be the case of 13 LAEs in the sample of Kulas et al. (2012) where there is a double-peak profile with similar heigh and a central notorious part.

Until now when single peaked profiles are present we associate this to the presence of inflows and outflows due to the asymmetry of the line , but in the case in which the profile have symmetry we could say that rotation in the principal effect governing the galaxy. For this reason a detailed study involving inflows/outflows and rotation kinematics would give as better understanding of the $Ly\alpha$ profiles we measured.

5. CONCLUSIONS

In this paper we have estimated the effects of gas bulk rotation on the emission of the Lyman α line. We based the study on the study of a simplified configuration of an homogeneous sphere rotating as a solid body. We explored a range of models by varying the rotation speed, hydrogen optical depth, dust optical depth and initial distribution of $Ly\alpha$ photons with respect to the gas density. This was implemented in CLARA, a Monte-Carlo radiative transfer code already used to study the Lyman α line.

As first we see how the width of the line changes using a modified FWHM explained in section 3.1, and we found that as gas bulk rotation increase also the width increase in a factor of $2 - 3$ in comparison with the static case. 'We also take into account the influence of the observer viewing angle, we found that observers with a line of sight perpendicular to the axis of rotation measure a 15% larger line width than those aligned with the rotation axis.'

As many observational spectra $Ly\alpha$ emission line (Kulas et al, Yamada et al) is double peaked, these peaks provide important information concerning gas kinematics and geometry, which can be partially explained with inflows/outflows of gas content. We study the effect of rotation in the position of this peaks, and we find that the position of the maxima does change with rotation for the homogeneous models when the double peak merged into a single peak as velocity increase. This effect is not seen for the central distribution when the double peak remains constant as the velocity increase. We also find that there is no dependency in the observer viewing angle
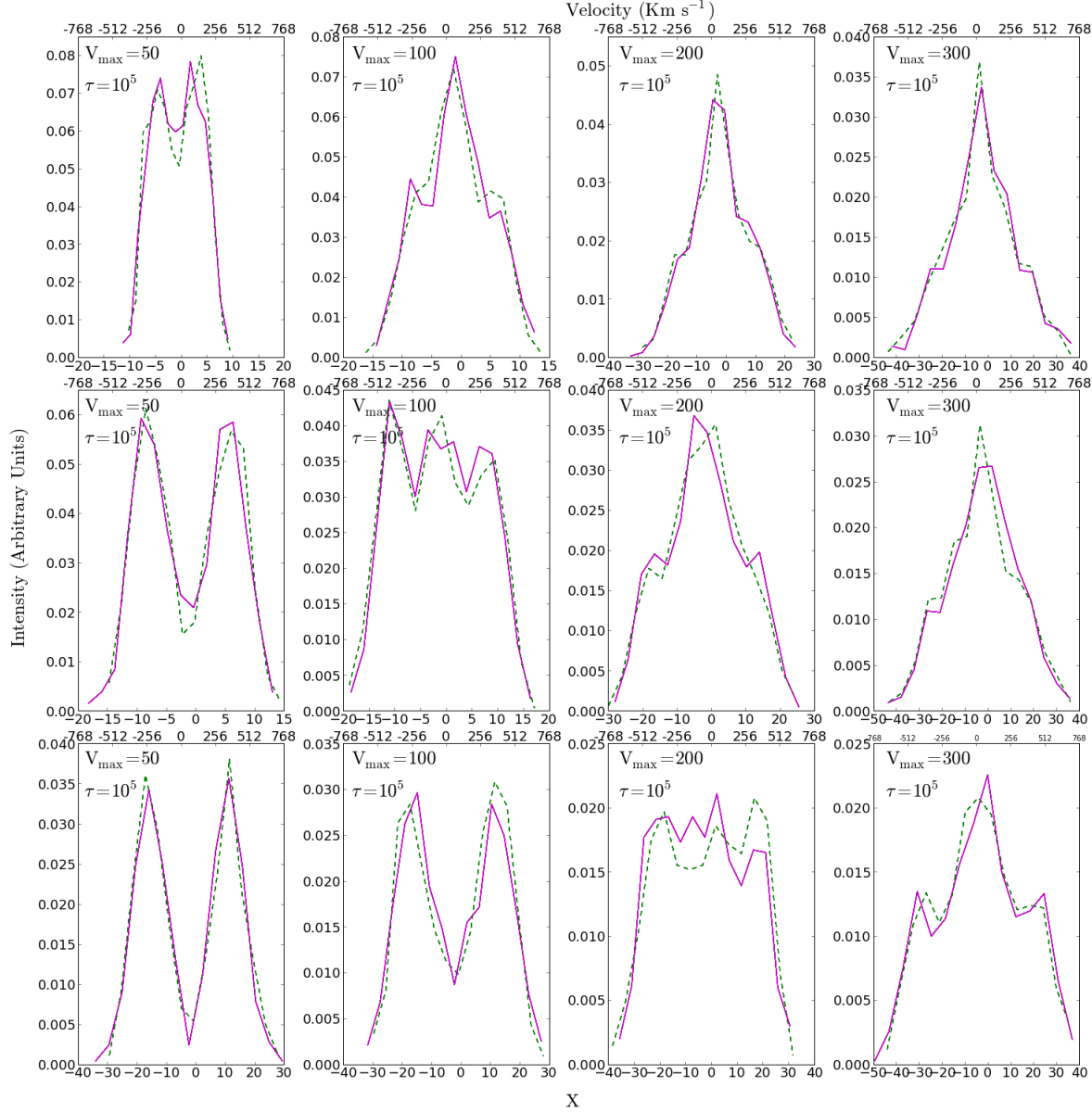
FIG. 10.— Off-center distribution Lyα profiles, off-center positions.

with the maxima position.

Concerning the escape fraction under rotational effects on the Lyα emission line, we found that the escape fraction increase in about $20\% - 30\%$ for the homogeneous sphere model. While rotational effects are negligible for the central models and the escape fraction remains constant. Also the observer viewing angle have no effect in the escape fraction neither for the homogeneous and central models. Complementing this analysis we study the average number of scatterings $< N_{scatt} >$ that photons

perform before escaping of the cloud taking into account rotational effects. The main result here is for the homogeneous models for which as velocity increase photons escape with about $\sim 39\%$ less scatterings than in the static case.

This paper illustrates for the first time the main effects of rotation in the morphology of the Lyα emission line, we estimate the range of this effects for simplified models.

REFERENCES

Adams, T. F. 1972, ApJ, 174, 439
Ahn, S.-H., Lee, H.-W., & Lee, H. M. 2000, Journal of Korean Astronomical Society, 33, 29
—. 2001, ApJ, 554, 604
Auer, L. H. 1968, ApJ, 153, 783
Avery, L. W., & House, L. L. 1968, ApJ, 152, 493

Barnes, L. A., Haehnelt, M. G., Tescari, E., & Viel, M. 2011, MNRAS, 416, 1723
Behrens, C., & Niemeyer, J. 2013, A&A, 556, A5
Dijkstra, M., Haiman, Z., & Spaans, M. 2006, ApJ, 649, 14
Dijkstra, M., & Kramer, R. 2012, MNRAS, 424, 1672

Forero-Romero, J. E., Yepes, G., Gottlöber, S., Knollmann, S. R., Cuesta, A. J., & Prada, F. 2011, MNRAS, 415, 3666

Forero-Romero, J. E., Yepes, G., Gottlöber, S., & Prada, F. 2012, MNRAS, 419, 952

Gawiser, E., Francke, H., Lai, K., Schawinski, K., Gronwall, C., Ciardullo, R., Quadri, R., Orsi, A., Barrientos, L. F., Blanc, G. A., Fazio, G., & Feldmeier, J. J. 2007, ApJ, 671, 278

Hansen, M., & Oh, S. P. 2006, MNRAS, 367, 979

Harrington, J. P. 1973, MNRAS, 162, 43

Koehler, R. S., Schuecker, P., & Gebhardt, K. 2007, A&A, 462, 7

Kulas, K. R., Shapley, A. E., Kollmeier, J. A., Zheng, Z., Steidel, C. C., & Hainline, K. N. 2012, ApJ, 745, 33

Laursen, P., Sommer-Larsen, J., & Andersen, A. C. 2009, ApJ, 704, 1640

Loeb, A., & Rybicki, G. B. 1999, ApJ, 524, 527

Neufeld, D. A. 1990, ApJ, 350, 216

Orsi, A., Lacey, C. G., & Baugh, C. M. 2012, MNRAS, 425, 87

Ouchi, M., Shimasaku, K., Akiyama, M., Simpson, C., Saito, T., Ueda, Y., Furusawa, H., Sekiguchi, K., Yamada, T., Kodama, T., Kashikawa, N., Okamura, S., Iye, M., Takata, T., Yoshida, M., & Yoshida, M. 2008, ApJS, 176, 301

Partridge, R. B., & Peebles, P. J. E. 1967, ApJ, 147, 868

Rhoads, J. E., Malhotra, S., Dey, A., Stern, D., Spinrad, H., & Jannuzi, B. T. 2000, ApJ, 545, L85

Schenker, M. A., Stark, D. P., Ellis, R. S., Robertson, B. E., Dunlop, J. S., McLure, R. J., Kneib, J.-P., & Richard, J. 2012, ApJ, 744, 179

Verhamme, A., Dubois, Y., Blaizot, J., Garel, T., Bacon, R., Devriendt, J., Guiderdoni, B., & Slyz, A. 2012, A&A, 546, A111

Verhamme, A., Schaerer, D., Atek, H., & Tapken, C. 2008, 111, 89

Verhamme, A., Schaerer, D., & Maselli, A. 2006, A&A, 460, 397

Yajima, H., Li, Y., Zhu, Q., Abel, T., Gronwall, C., & Ciardullo, R. 2012, ApJ, 754, 118

Yamada, T., Nakamura, Y., Matsuda, Y., Hayashino, T., Yamauchi, R., Morimoto, N., Kousai, K., & Umemura, M. 2012, AJ, 143, 79

Zheng, Z., & Miralda-Escudé, J. 2002, ApJ, 578, 33

Zheng, Z., & Wallace, J. 2013, ArXiv e-prints